

Hybrid Representation Learning via Epistemic Graph

Jin Yuan
Southeast University
Nanjing

Yang Zhang
Lenovo Research
Beijing

Yangzhou Du
Lenovo Research
Beijing

Zhongchao Shi
Lenovo Research
Beijing

Xin Geng*
Southeast University
Nanjing

Jianping Fan
Lenovo Research
Beijing

Yong Rui*
Lenovo Research
Beijing

Abstract

In recent years, deep models have achieved remarkable success in many vision tasks. Unfortunately, their performance largely depends on intensive training samples. In contrast, human beings typically perform hybrid learning, e.g., spontaneously integrating structured knowledge for cross-domain recognition or on a much smaller amount of data samples for few-shot learning. Thus it is very attractive to extend hybrid learning for the computer vision tasks by seamlessly integrating structured knowledge with data samples to achieve more effective representation learning. However, such a hybrid learning approach remains a great challenge due to the huge gap between the structured knowledge and the deep features (learned from data samples) on both dimensions and knowledge granularity. In this paper, a novel Epistemic Graph Layer (EGLayer) is developed to enable hybrid learning, such that the information can be exchanged more effectively between the deep features and a structured knowledge graph. Our EGLayer is composed of three major parts: (a) a local graph module to establish a local prototypical graph through the learned deep features, i.e., aligning the deep features with the structured knowledge graph at the same granularity; (b) a query aggregation model to aggregate useful information from the local graphs, and using such representations to compute their similarity with global node embeddings for final prediction; and (c) a novel correlation loss function to constrain the linear consistency between the local and global adjacency matrices. EGLayer is a plug-and-play module that can replace the standard linear classifier, significantly improving the performance of deep models. Extensive experiments have demonstrated that EGLayer can greatly enhance representation learning for the tasks of cross-domain

recognition and few-shot learning, and the visualization of knowledge graphs can aid in model interpretation.

1. Introduction

Over the past decade, deep models have attained significant achievements in many vision tasks. However, their success largely hinges on huge amounts of data samples and complicated model architectures [4, 8, 11, 62]. In contrast, human beings typically perform hybrid learning, e.g., spontaneously integrating structured knowledge with a much smaller amount of data samples to achieve more effective representation learning, and can thus easily achieve cross-domain recognition. Therefore, it is very attractive to extend such hybrid learning for the computer vision tasks by seamlessly integrating structured knowledge with data samples to achieve more effective representation learning. However, such a hybrid learning approach remains a great challenge due to the huge gap between the structured knowledge and the deep features (learned from data samples) on both dimensions and knowledge granularity.

Graph has provided a direct and intuitive approach to represent structured knowledge. In a graph, each node represents one specific entity, while the relationship between the entities is represented by the edge adjacency matrix. Compared with conventional knowledge fusion methods [1, 2, 3, 17, 20, 24], graph-based methods have two distinct advantages: 1. Node embeddings could represent general concept of an entity with ample knowledge; 2. By concentrating on relational adjacency matrix, the graph representation is intuitively closer to humans' structured knowledge.

One critical challenge for hybrid learning (e.g., incorporating knowledge graph into data-driven deep learning) is the mismatch between deep features (learned from data samples) and graph representations of structured knowl-

¹Corresponding authors.

edge. Such mismatch can be divided into two parts: firstly, the deep features typically represent the visual distribution of a single image, while the structured graph contains the overall semantic knowledge which commonly share among many images, i.e., their information granularities are significantly different. Secondly, the deep features are usually in high dimensions, while the structured knowledge graph is a set of nodes and edges with much lower dimensions. Existing methods [6, 10, 26, 29, 37] mostly rely on a simple linear mapping or matrix multiplication to merge them, which could be ineffective and unstable.

To address the mismatch issue on information granularity, we propose a hybrid learning method with a local graph module, which establishes dynamic update of a local prototypical graph by historical deep features. This module acts as a memory bank and transfers deep features to the holistic visual graph. We then devise a query aggregation model that injects the current deep feature to the local graph and uses a Graph Neural Network (GNN) [18, 23, 55] to aggregate information for both the local graph node and feature node, aligning them to the same dimension as the global graph. The final prediction is performed based on the similarity between the knowledge-enhanced deep features and the global node embeddings. Moreover, a novel correlation loss function is developed to maintain linear consistency between the local graph and the global one by constraining the adjacency matrix. Together, these three parts constitute a well functional Epistemic Graph Layer (EGLayer).

The EGLayer is a versatile plug-and-play module that can be easily integrated into most existing deep models in the place of a standard linear classifier. Our experiments on the computer vision tasks of cross-domain recognition and few-shot learning have demonstrated the effectiveness of our proposed hybrid learning approach with such EGLayer, which achieves significant improvements on both performance and robustness. Moreover, such EGLayer has also shown promising results compared with conventional knowledge integration methods. Finally, the visualization of the local graphs and the global ones can provide valuable insights for model interpretation.

2. Related Works

Research on integrating human knowledge into deep models using graphs has drawn significant attention in recent years, which can be mainly categorized into two streams: visual guided graph representation learning and knowledge graph guided visual feature learning.

2.1. Visual Guided Graph Representation Learning

In this direction, research [6, 10, 16, 22, 41, 59] often involve taking a fixed visual feature extractor and designing a function to transform graph embeddings to visual features, which are then fused together. Wang et al. [59] construct

a Graph Convolutional Network (GCN) using the WordNet structure and train it to predict visual classifiers pre-trained on ImageNet. By leveraging the relationships learned by GCN, it is able to transfer knowledge to new class nodes and perform zero-shot learning. Subsequently, Peng et al. [41] improve their works by presenting knowledge transfer network, which replaces the inner product with cosine similarity of images. Moreover, Chen et al. [6] propose a knowledge graph transfer network, which freezes the visual feature extractor and adopts three distance metrics to measure the similarity of visual features.

2.2. Knowledge Graph Guided Visual Feature Learning

Other works [29, 35, 38, 44, 51, 66] commonly focus on knowledge graph guided visual feature learning, as knowledge graph is considered more reliable than visual features. These works usually treat the knowledge graph as either a fixed external knowledge base or a high-level supervision to visual features. Socher et al. [51] utilize a combination of dot-product similarity and hinge rank loss to learn a linear transformation function between the visual embedding space and the semantic embedding space to avoid the fails in high dimensional space. More important, Zhang et al. [66] propose a semantic similarity embedding method by representing target data instances as a combination of a certain proportion of seen classes. They create a semantic space where each novel class can be expressed as a probability mixture of the projected source attribute vectors of the known classes. Recently, Monka et al. [35] adopt knowledge graph to train a visual feature extractor by using contrastive knowledge graph embedding loss, which outperforms conventional methods.

To our best knowledge, existing works hardly make efforts on aligning the knowledge granularity between local image features and the global graph. Consequently, they usually suffer from inefficient knowledge fusion issues and under-utilize the knowledge embedded in the graph. Such an observation drives us to explore a reliable and flexible knowledge graph projection method.

3. Method

For a typical classification task, we have a dataset $\mathcal{D} = (\mathbf{x}, \mathbf{y})$ to train a model, where \mathbf{x} represents input images and \mathbf{y} represents their respective labels. We firstly form the typical process of the classification task.

Firstly, we exploit a feature extractor f_θ to extract image features $\mathbf{X} \in \mathbb{R}^D$ from \mathbf{x} , where θ represents the learnable parameters. The formula can be written as:

$$\mathbf{X} = f_\theta(\mathbf{x}). \quad (1)$$

Then, a classifier is utilized to compute the probability

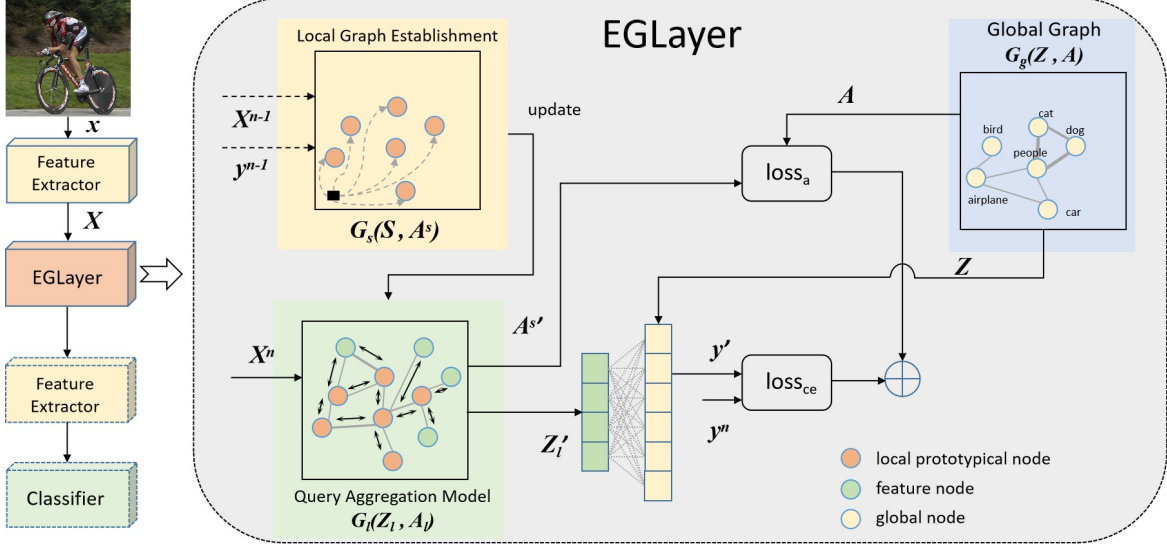


Figure 1. This figure illustrates the general framework of our proposed Epistemic Graph Layer. It can be inserted after any feature extractor layer to transfer the image feature dimension and granularity. In this paper, we primarily focus on replacing the standard linear classifier.

of each category given the feature:

$$y' = \mathbf{W} \mathbf{X}. \quad (2)$$

Finally, the optimized function between y' and y is:

$$\mathcal{L} = loss_{ce}(\mathbf{y}, \mathbf{y}'), \quad (3)$$

where cross-entropy loss is often used in classification task.

Except for the labels of each instance, there are additional knowledge graph available during model training. Assuming we have a global knowledge graph G_g , the critical problem is how to integrate it to facilitate model training.

We define $G_g = (\mathbf{Z}, \mathbf{A})$, where $\mathbf{Z} \in \mathbb{R}^{n \times d}$ represents the n nodes with d -dimensional features, and $\mathbf{A} \in \mathbb{R}^{n \times n}$ denotes the edges among the n nodes.

3.1. Linear Projection Layer

To integrate the knowledge graph G_g into model training, the first step is to project the visual features to the same dimension as the graph nodes. The most straightforward approach is using a linear layer:

$$\mathbf{Z}' = \mathbf{W}_p \mathbf{X}, \quad (4)$$

where $\mathbf{W}_p \in \mathbb{R}^{d \times D}$ denotes the learnable mapping matrix.

Next, we can calculate the cosine similarity between \mathbf{Z}' and the global graph node embedding \mathbf{Z}_i :

$$y' = \frac{\exp(\langle \mathbf{Z}', \mathbf{Z}_i \rangle)}{\sum_n \exp(\langle \mathbf{Z}', \mathbf{Z}_i \rangle)}, \quad (5)$$

where $\langle \cdot, \cdot \rangle$ represents the cosine similarity of two vectors.

3.2. Epistemic Graph Layer

To achieve an efficient interaction between local features and prior knowledge, we propose a novel EGLayer, which is composed of three major parts. Firstly, the local graph module establishes a dynamically updated prototypical graph by historical features. This module transfers the instance-level features to the graph-level representation, acting as a memory bank. Secondly, in the query aggregation model, the extracted features are injected into the obtained local graph to generate the query graph, which is further fed into a GNN to aggregate information for both feature and local graph nodes. In this manner, we fulfill a natural dimension alignment between the local and global graphs and obtain the prediction logits. Finally, we propose an auxiliary correlation loss by constraining the local and global adjacency matrices, further ensuring linear consistency and comparable knowledge granularity between the local and global graphs. The overall framework is shown in Figure 4.

3.2.1 Local Graph Establishment

To align visual features with the global graph, we first establish a local graph $G_l = (\mathbf{Z}_l, \mathbf{A}_l)$ by the extracted features.

We define \mathcal{D}_k as the set of k -th category samples. The local prototype can be obtained by averaging the features of the categories:

$$\mathbf{S}'_k = \frac{1}{|\mathcal{D}_k|} \sum_{(\mathbf{x}_i, \mathbf{y}_i) \in \mathcal{D}_k} f_{\theta}(\mathbf{x}_i) \quad (6)$$

To dynamically maintain the local prototype, we leverage exponential moving average scheme [5, 21, 58, 63] to update $\mathbf{S}_k \in \mathbb{R}^D$ in each iteration:

$$\mathbf{S}_k = \beta \mathbf{S}_k + (1 - \beta) \mathbf{S}'_k \quad (7)$$

The local prototype \mathbf{S} represents the node embeddings of the local graph, which serves as a memory bank that preserves historical visual features, aligning the granularity of the local graph with the semantic global graph.

To facilitate the interaction between the extracted feature and local graph, we build the updated local graph embedding \mathbf{Z}_l :

$$\mathbf{Z}_l = [\underbrace{\mathbf{S}_1 \mathbf{S}_2 \cdots \mathbf{S}_n}_{\text{local prototypes}} \underbrace{\mathbf{X}_1 \mathbf{X}_2 \cdots \mathbf{X}_q}_{\text{query samples}}]^T. \quad (8)$$

3.2.2 Query Aggregation Model

To align the local graph with global graph in the same dimensional space, we utilize GNNs via the aggregation operator. Before the aggregation process, we need to define the adjacency matrix \mathbf{A}_l . For each local prototype \mathbf{S} in the \mathbf{G}_l , it is expected to aggregate information from highly related local graph nodes. We compute the adjacency matrix \mathbf{A}^s using the Gaussian kernel \mathcal{K}_G [32, 58, 63]:

$$\mathbf{A}_{i,j}^s = \mathcal{K}_G \left(\mathbf{S}_i^T, \mathbf{S}_j^T \right) = \exp \left(-\frac{\left\| \mathbf{S}_i^T - \mathbf{S}_j^T \right\|_2^2}{2\sigma^2} \right), \quad (9)$$

where σ is a hyperparameter to control the sparsity of \mathbf{A}^s that is set as 0.05 by default. Moreover, \mathbf{A}^s is a symmetric matrix ($\mathbf{A}_{i,j}^s = \mathbf{A}_{j,i}^s$), so each node can both aggregate and transfer information.

The query node \mathbf{X} also needs to aggregate useful information from the prototypical nodes, and the unidirectional aggregation matrix \mathbf{A}^{xs} is defined as:

$$\mathbf{A}_{i,j}^{xs} = \mathcal{K}_G \left(\mathbf{S}_i^T, \mathbf{X}_j^T \right) = \exp \left(-\frac{\left\| \mathbf{S}_i^T - \mathbf{X}_j^T \right\|_2^2}{2\sigma^2} \right). \quad (10)$$

Subsequently, we calculate the adjacency matrix \mathbf{A}_l :

$$\mathbf{A}_l = \begin{bmatrix} \mathbf{A}^s & \mathbf{A}^{xs} \\ \mathbf{A}^{xsT} & \mathbf{E} \end{bmatrix}, \quad (11)$$

where \mathbf{E} represents the identity matrix since query features are not allowed to interact information with each other.

With the local graph embedding \mathbf{Z}_l and adjacency matrix \mathbf{A}_l , we exploit GCN [13, 23] to conduct the aggregation operation:

$$\mathbf{H}^{(m+1)} = \sigma \left(\tilde{\mathbf{D}}_l^{-\frac{1}{2}} \tilde{\mathbf{A}}_l \tilde{\mathbf{D}}_l^{-\frac{1}{2}} \mathbf{H}^{(m)} \mathbf{W}^{(m)} \right), \quad (12)$$

where $\tilde{\mathbf{A}}_l$ is the local correlation matrix \mathbf{A}_l with self-connections, and $\tilde{\mathbf{D}}_l$ is the degree matrix of $\tilde{\mathbf{A}}_l$. $\mathbf{W}^{(m)}$ denotes the learnable matrix in m -th layer, while σ is the activation function. Here, we take the local graph embedding \mathbf{Z}_l as the first layer input of $\mathbf{H}^{(m)}$, and the final aggregated node representation $\mathbf{H}^{(m+1)}$ are defined as \mathbf{Z}'_l .

Finally, we exploit Eq. 5 to calculate the final predictions by \mathbf{Z}'_l and global node embedding \mathbf{Z} .

3.2.3 Correlation Loss Function

To obtain adequate and consistent guidance by global graph, we here intentionally constrain the local adjacency matrix. However, the local adjacency matrix is fixed in each training iteration since \mathbf{A}^s is only related to the local graph embedding \mathbf{S} , which is updated in advance of each iteration. Therefore, we introduce an extra trainable matrix \mathbf{W}_a for \mathbf{A}^s to get the amended adjacency matrix in local graph:

$$\mathbf{A}_{i,j}^{s'} = \mathbf{W}_a \mathbf{A}_{i,j}^s = \mathbf{W}_a \mathcal{K}_G \left(\mathbf{S}_i^T, \mathbf{S}_j^T \right). \quad (13)$$

Then, the adjacency matrix in Eq. 11 can be finalized as:

$$\mathbf{A}_l = \begin{bmatrix} \mathbf{A}^{s'} & \mathbf{A}^{xs} \\ \mathbf{A}^{xsT} & \mathbf{E} \end{bmatrix}. \quad (14)$$

Accordingly, we can build an auxiliary loss function:

$$\mathcal{L} = loss_{ce}(\mathbf{y}, \mathbf{y}') + \lambda loss_a(\mathbf{A}, \mathbf{A}^{s'}), \quad (15)$$

where $loss_a$ could be any distance function like l_1 and l_2 distances, and λ is a hyper-parameter empirically set as 0.1.

4. Experiments

As discussed before, our proposed EGLayer is a plug-and-play module that can benefit most kinds of deep models by conveniently replacing their standard classifiers. In order to examine the effectiveness of our knowledge guidance and extrapolation, we mainly focused on several challenging tasks, including cross-domain classification, universal domain adaptation, and few-shot learning.

The establishment of the global knowledge graph has various available scheme. The co-occurrence graph [10, 12, 60] represents the frequency of two classes occurring together, but is not suitable for single-label tasks and heavily depends on the size of the dataset. Another option is the pre-defined knowledge graph [25, 30, 31, 54, 61], which is constructed using manually labeled relational datasets or knowledge base. In our approach, we adopt a simpler solution by utilizing the word embeddings from GloVe [42] and Eq. 9 to obtain node embeddings and adjacency matrices, which is an adaptive approach that does not require additional sources of knowledge.

Table 1. Comparison experiments on Office-31 dataset

Methods	A→W	D→W	W→D	A→D	D→A	W→A	Average
ResNet50	65.41	79.25	91.00	70.00	44.68	50.38	66.79
ResNet50 + LPLayer	67.92	85.53	94.00	71.00	53.62	56.22	71.38
ResNet50 + EGLayer	72.96	94.34	98.00	76.00	55.18	60.06	76.09

Table 2. Comparison experiments on Office-Home dataset

Methods	A→C	A→P	A→R	C→A	C→P	C→R	P→A	P→C	P→R	R→A	R→C	R→P	Average
ResNet50	40.42	59.48	69.10	45.07	56.55	60.13	39.71	39.86	68.09	58.64	43.60	73.64	54.52
ResNet50 + LPLayer	40.78	28.69	66.43	40.48	32.88	43.04	56.68	44.81	69.03	65.08	49.79	52.58	49.19
ResNet50 + EGLayer	42.84	61.62	66.72	47.42	58.58	58.18	51.80	40.51	68.21	65.36	46.72	74.07	56.84

4.1. Cross-Domain Classification

4.1.1 Datasets

In this experiment, we train the model on the source domain and then perform classification directly on the target domain without using any target domain data. We conduct experiments on two benchmark datasets, namely Office-31 [48] and Office-Home [56]. The Office-31 dataset consists of 4,652 images from 31 categories and is divided into three domains: *Amazon* (A), *Dslr* (D), and *Webcam* (W). The Office-Home dataset has 15,500 images with 65 categories and is divided into four domains: *Art* (A), *Clipart* (C), *Product* (P), and *Real World* (R).

4.1.2 Comparison Results

Table 1 and Table 2 present the results of our experiments with different model settings. ResNet50 [19] refers to ResNet50 backbone with a standard linear classifier. ResNet50 + LPLayer denotes the ResNet50 backbone with the linear projection layer described in Section 3.1. ResNet50 + EGLayer is the ResNet50 backbone equipped with our proposed epistemic graph layer. The only difference among the three models is the classifier, which allows us to make a fair comparison.

On average, ResNet50 + LPLayer outperforms ResNet50 by 4.59% on Office-31, and our ResNet50 + EGLayer further yields a 4.69% performance gain and obtains the best results in all cases. Unexpectedly, ResNet50 + LPLayer shows an obvious performance drop on Office-Home by 5.33%, which could be attributed to its insufficient knowledge integration. In contrast, our proposed ResNet50 + EGLayer achieves a remarkable improvement by 2.32%. Specifically, the largest margin is reported in the D→W task on Office-31, where ResNet50 + EGLayer improves the results from 79.25% to 94.34%, an impressive increase of 15.09%. These results suggest the proposed EGLayer learns a better representation.

4.1.3 Visualization of Graphs

We visualize two graphs including enhanced local graph and global graph. To show the results clearly, we only show the top-150 edges of strong relationship, and the thicker edge represents the higher relational edge value (See Appendix for more details).

The enhanced local graph mainly contains knowledge from visual sources, while the global graph consists of more semantic knowledge. As shown in Figure 2, we highlight two typical nodes. The *Scissors* node in the global graph is close to two types of concepts, tools and stationeries. The typical tools include *Knives*, *Hammer*, and *Screwdriver*, while the stationeries contain *Eraser*, *Pencil*, and *Pen*. In the enhanced local graph, *Scissors* is only related to the typical tools category due to their similar metallic appearance. Another interesting node is *Lamp Shade*, which is highly related to the *Desk Lamp* since the *Lamp Shade* image is always combined with the lamp. On the contrary, these two nodes do not have an edge in the global graph, which may be attributed to the semantic emphasis of *Lamp Shade* as a shade rather than a lamp.

4.2. Open-Set Domain Adaptation

4.2.1 Implementation Details

In this subsection, we conduct experiments on open-set domain adaptation tasks, where the source and target domains have some shared and some private categories. We adopt the task definition proposed in [64]. Specifically, we denote the label sets of the source and target domains as \mathcal{C}_s and \mathcal{C}_t , respectively, and $\mathcal{C} = \mathcal{C}_s \cap \mathcal{C}_t$ represents the set of shared categories. Furthermore, $\bar{\mathcal{C}}_s = \mathcal{C}_s \setminus \mathcal{C}$ and $\bar{\mathcal{C}}_t = \mathcal{C}_t \setminus \mathcal{C}$ represent the private categories in the source and target domains, respectively. We can then quantify the commonality between the two domains as $\xi = \frac{|\mathcal{C}_s \cap \mathcal{C}_t|}{|\mathcal{C}_s \cup \mathcal{C}_t|}$.

For the Office-31 dataset, we choose 10 categories as shared categories \mathcal{C} , the following 10 categories as source private categories \mathcal{C}_s , and the remaining categories as target private categories \mathcal{C}_t . For the Office-Home dataset, we take the first 10 categories as \mathcal{C} , the next 5 categories \mathcal{C}_s , and the

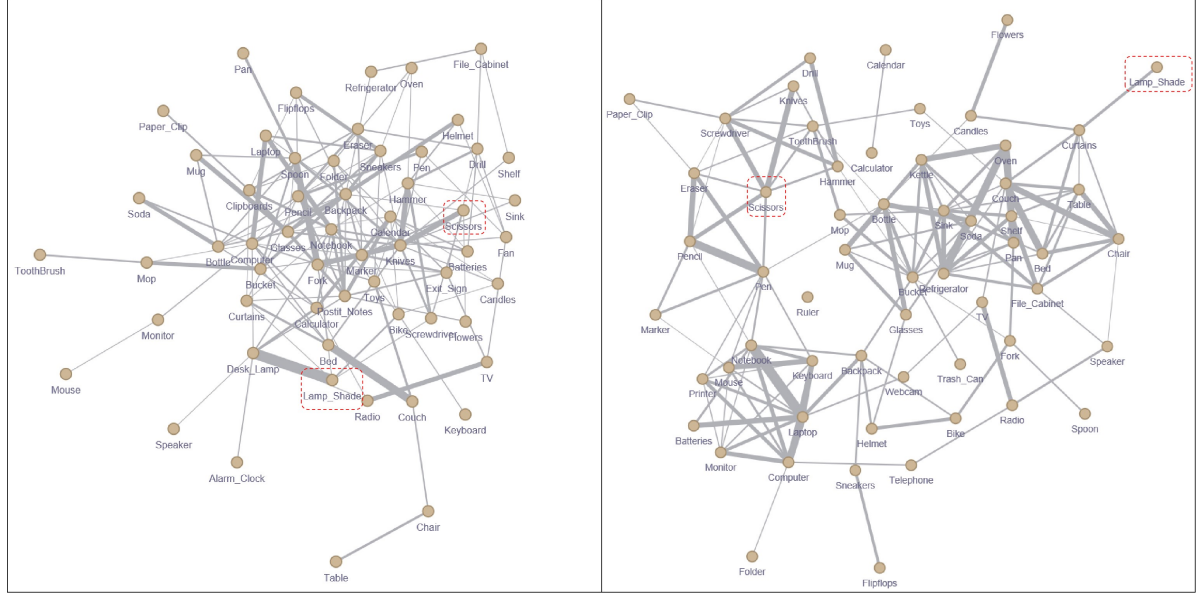


Figure 2. The left visualized graph is enhanced local graph, and the right is global graph. These experiments are conducted in Office-Home datasets of 65 classes in *Clipart* domain. We have highlighted two typical nodes: the *Lamp Shade* is visually similar to *Desk Lamp* while the *Scissors* is semantically closer to stationery objects.

Table 3. Universal domain adaptation experiments on Office-31 dataset

Methods	A→W	D→W	W→D	A→D	D→A	W→A	Average
DANN [15]	80.65	80.94	88.07	82.67	74.82	83.54	81.78
RTN [33]	85.70	87.80	88.91	82.69	74.64	83.26	84.18
IWAN [65]	85.25	90.09	90.00	84.27	84.22	86.25	86.68
PADA [65]	85.37	79.26	90.91	81.68	55.32	82.61	79.19
ATI [40]	79.38	92.60	90.08	84.40	78.85	81.57	84.48
OSBP [49]	66.13	73.57	85.62	72.92	47.35	60.48	67.68
UAN [64]	77.16	94.54	95.48	78.71	84.47	82.14	85.42
UAN + LPLayer	83.69	91.20	95.17	84.90	84.93	84.24	87.36
UAN + EGLayer	83.39	92.86	94.70	84.50	87.61	86.69	88.29

rest as \mathcal{C}_t . As a result, we obtain ξ values of 0.32 and 0.15 for the Office-31 and Office-Home datasets, respectively.

4.2.2 Comparison Results

We summarize the results in Table 8 and Table 4. To thoroughly understanding the effect of knowledge integration, we replace the linear classifier in UAN [64] with LPLayer and EGLayer, namely UAN + LPLayer and UAN + EGLayer respectively.

In the open-world setting, integrating knowledge is a crucial factor of performance promotion. On average, UAN + LPLayer brings stable 1.94% and 1.61% improvements over vanilla UAN on Office-31 and Office-Home datasets. The proposed UAN + EGLayer further enhances the results by 0.93% and 0.1% in comparison to UAN + LPLayer, which demonstrates that EGLayer has a better generalization ca-

pability than conventional linear knowledge fusion. Interestingly, we observe that both knowledge-based methods obtain more significant improvements in challenging tasks (i.e. tasks with low accuracy), such as A→W and A→D. In general, UAN + EGLayer beats all competitors and reaches state-of-the-art performance in open-world setting.

4.2.3 Correlation Loss Study

We conduct experiments for λ in Eq. 15. We trained model with λ of 0, 0.01, 0.05, 0.1, 0.5, 1, and 5 for 6,000 iterations. Specifically, we set λ as 0 for ablation study. The results on validation set of *art* to *clipart* is shown Figure 3.

We observe that all experimental settings reach their peak performance at around 5,500 iterations. The settings with values of 0, 1, and 5 perform relatively poor, with results lower than 65.7%. On the other hand, the remaining

Table 4. Universal domain adaptation experiments on Office-Home dataset

Methods	A→C	A→P	A→R	C→A	C→P	C→R	P→A	P→C	P→R	R→A	R→C	R→P	Average
DANN [15]	56.17	81.72	86.87	68.67	73.38	83.76	69.92	56.84	85.80	79.41	57.26	78.26	73.17
RTN [33]	50.46	77.80	86.90	65.12	73.40	85.07	67.86	45.23	85.50	79.20	55.55	78.79	70.91
IWAN [65]	52.55	81.40	86.51	70.58	70.99	85.29	74.88	57.33	85.07	77.48	59.65	78.91	73.39
PADA [65]	39.58	69.37	76.26	62.57	67.39	77.47	48.39	35.79	79.60	75.94	44.50	78.10	62.91
ATI [40]	52.90	80.37	85.91	71.08	72.41	84.39	74.28	57.84	85.61	76.06	60.17	78.42	73.29
OSBP [49]	47.75	60.90	76.78	59.23	61.58	74.33	61.67	44.50	79.31	70.59	54.95	75.18	63.90
UAN [64]	65.92	79.82	88.09	71.99	75.11	84.54	77.56	64.16	89.06	81.92	65.87	83.80	77.32
UAN + LPLayer	67.43	81.64	88.97	76.19	81.58	87.29	79.86	63.11	88.73	79.70	68.62	84.07	78.93
UAN + EGLayer	65.64	82.65	90.48	80.73	80.44	87.32	79.57	63.85	88.68	79.77	63.99	85.18	79.03

Table 5. Comparison with state-of-the-art methods on miniImageNet dataset.

Methods	Backbone	1-shot	5-shot
Matching Networks [57]	ConvNet-4	43.56 ± 0.84	55.31 ± 0.73
Activation to Parameter [43]	WRN-28-10	59.60 ± 0.41	73.74 ± 0.19
LEO [47]	WRN-28-10	61.76 ± 0.08	77.59 ± 0.12
Baseline++ [7]	ResNet-18	51.87 ± 0.77	75.68 ± 0.63
Prototypical Networks [50]	ResNet-12	53.81 ± 0.23	75.68 ± 0.17
SNAIL [34]	ResNet-12	55.71 ± 0.99	68.88 ± 0.92
AdaResNet [36]	ResNet-12	56.88 ± 0.62	71.94 ± 0.57
TADAM [39]	ResNet-12	58.50 ± 0.30	76.70 ± 0.30
MTL [52]	ResNet-12	61.20 ± 1.80	75.50 ± 0.80
MetaOptNet [27]	ResNet-12	62.64 ± 0.61	78.63 ± 0.46
ProtoNets + TRAML [28]	ResNet-12	60.31 ± 0.48	77.94 ± 0.57
Classifier-Baseline [9]	ResNet-12	58.91 ± 0.23	77.76 ± 0.17
Meta-Baseline [9]	ResNet-12	63.17 ± 0.23	79.26 ± 0.17
Classifier-Baseline + LPLayer	ResNet-12	60.96 ± 0.23	78.07 ± 0.17
Classifier-Baseline + EGLayer	ResNet-12	61.11 ± 0.28	78.84 ± 0.21
Meta-Baseline + LPLayer	ResNet-12	62.27 ± 0.23	77.63 ± 0.17
Meta-Baseline + EGLayer	ResNet-12	63.55 ± 0.26	79.78 ± 0.54

Table 6. Comparison with state-of-the-art methods on tieredImageNet dataset

Methods	Backbone	1-shot	5-shot
MAML [14]	ConvNet-4	51.67 ± 1.81	70.30 ± 1.75
Prototypical Networks [50]	ConvNet-4	53.31 ± 0.89	72.69 ± 0.74
Relation Networks [53]	ConvNet-4	54.48 ± 0.93	71.32 ± 0.78
LEO [47]	WRN-28-10	66.33 ± 0.05	81.44 ± 0.09
MetaOptNet [27]	ResNet-12	65.99 ± 0.72	81.56 ± 0.53
Classifier-Baseline [9]	ResNet-12	68.07 ± 0.26	83.74 ± 0.18
Meta-Baseline [9]	ResNet-12	68.62 ± 0.27	83.74 ± 0.18
Classifier-Baseline + LPLayer	ResNet-12	68.28 ± 0.26	83.04 ± 0.18
Classifier-Baseline + EGLayer	ResNet-12	69.38 ± 0.53	84.38 ± 0.55
Meta-Baseline + LPLayer	ResNet-12	69.16 ± 0.56	82.64 ± 0.41
Meta-Baseline + EGLayer	ResNet-12	69.41 ± 0.55	83.74 ± 0.58

four settings perform better than 66.0%. Among them, the setting with $\lambda = 0.1$ achieves the highest performance of 66.23%. Thus, we set λ as 0.1 in Eq. 15. Furthermore, the best setting for λ yields a performance gain of about 0.5% compared to the version without correlation loss, demonstrating the effectiveness of this correlation loss.

4.3. Few-Shot Learning

4.3.1 Datasets

We evaluate the few-shot learning performance of EGLayer on two datasets. The miniImageNet [57] is sampled from ImageNet [46] of 100 classes. 64 classes are used for training, the rest 16 and 20 classes are used for validation and

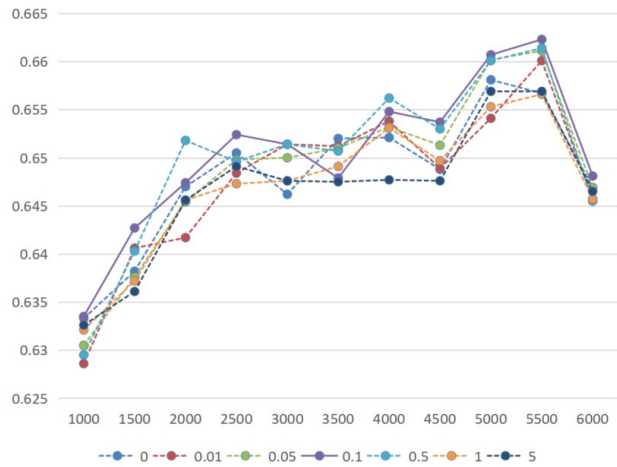
Comparison results under different λ 

Figure 3. The results of the comparison are presented under varying values of λ . The validation results demonstrate that $\lambda = 0.1$ yields the best performance as compared to higher and lower values of λ . Additionally, the proposed method with correlation loss ($\lambda = 0.1$) outperforms the method without correlation loss ($\lambda = 0$).

testing, respectively. Each class contains 600 images resized to 84×84 resolution. The tieredImageNet [45] is a larger datasets consisting of 608 classes sampled from ImageNet [46] too. All classes are divided 351, 97, 160 classes for training, validation and testing. Different from miniImageNet, tieredImageNet is more challenging owing to the long semantic distance between base and novel classes.

4.3.2 Implementation Details

We mainly follow the previous works [9, 27, 39] to test our methods. SGD optimizer is exploited with a 0.1 learning rate, 0.1 decay factor and momentum 0.9. The whole model is trained 120 epoch with ResNet-12 backbone.

Our methods are evaluated based on the Classifier-Baseline and Meta-Baseline proposed in [9]. These baselines first utilize the whole label-set for training on all base classes with cross-entropy loss. For validation, classifier is removed and feature extractor f_θ is used to computes the

Table 7. Transfer experiments on miniImageNet and tieredImageNet

dataset	Methods	Backbone	1-shot	5-shot
miniImageNet→tieredImageNet	Classifier-Baseline	ResNet-12	64.15 ± 0.54	79.81 ± 0.42
	Classifier-Baseline + LPLayer	ResNet-12	64.51 ± 0.33	79.83 ± 0.44
	Classifier-Baseline + EGLayer	ResNet-12	64.50 ± 0.55	79.94 ± 0.43
	Meta-Baseline	ResNet-12	67.63 ± 0.49	80.99 ± 0.42
	Meta-Baseline + LPLayer	ResNet-12	67.61 ± 0.58	80.88 ± 0.43
	Meta-Baseline + EGLayer	ResNet-12	67.98 ± 0.59	81.27 ± 0.43
tieredImageNet→miniImageNet	Classifier-Baseline	ResNet-12	76.35 ± 0.22	90.50 ± 0.12
	Classifier-Baseline + LPLayer	ResNet-12	76.66 ± 0.24	90.23 ± 0.12
	Classifier-Baseline + EGLayer	ResNet-12	77.39 ± 0.28	91.11 ± 0.14
	Meta-Baseline	ResNet-12	76.79 ± 0.24	89.53 ± 0.13
	Meta-Baseline + LPLayer	ResNet-12	78.24 ± 0.29	90.41 ± 0.22
	Meta-Baseline + EGLayer	ResNet-12	77.90 ± 0.26	90.42 ± 0.15

average embedding w_c of each class c in support-set \mathcal{D}^S :

$$w_c = \frac{1}{|\mathcal{D}_c^S|} \sum_{x \in \mathcal{D}_c^S} f_\theta(x). \quad (16)$$

Then, for a query sample x , cosine similarity is computed between the extracted features of x and average embedding w_c for the final prediction:

$$p(y = c | x) = \frac{\exp(\tau \cdot \langle f_\theta(x), w_c \rangle)}{\sum_{c'} \exp(\tau \cdot \langle f_\theta(x), w_{c'} \rangle)}, \quad (17)$$

where the Meta-Baseline trains a learnable scalar τ through a meta learning way and the Classifier-Baseline fixes the τ as 1.0.

We simply replace the classifier layers in both baselines, namely as Classifier-Baseline + EGLayer and Meta-Baseline + EGLayer, respectively. We also compare with Classifier-Baseline + LPLayer and Meta-Baseline + LPLayer to show the superior knowledge integration capability of the EGLayer.

4.3.3 Comparison Results

We compare our proposed method with current state-of-the-art methods in Table 5 and Table 6. All results are average of 5-way accuracy with 95% confidence interval.

For miniImageNet, Classifier-Baseline + LPLayer holds a clear advantage in 1-shot settings, which verifies our assumption that integrating knowledge facilitates visual features converging to semantic space. Classifier-Baseline + EGLayer further obtains stable improvements in both 1-shot and 5-shot results. On the other hand, inserting a LPLayer to the Meta-Baseline even causes a slight performance decline in both 1-shot and 5-shot results. In comparison, our proposed EGLayer has always maintained a

performance gain, demonstrating its adaptability and effectiveness. Moreover, we observe a significant difference between Classifier-Baseline and Meta-Baseline in 1-shot settings, while integrating knowledge largely bridges this gap, making the model more stable.

For tieredImageNet, we notice that the performance difference between Classifier-Baseline and Meta-Baseline becomes much smaller, which may be attributed to more samples and classes adopted. Compared with LPLayer, EGLayer enables a more adequate and reliable knowledge injection and achieves significant advantages in both settings. In detail, the Classifier-Baseline + EGLayer performs the state-of-the-art results in 5-shot experiments with 84.38%, and the Meta-Baseline + EGLayer reaches the top performance in 1-shot experiments with 69.41%. Both are highly competitive results compared to prior works.

4.3.4 Transfer Learning

We have evaluated the transfer learning ability of our method by exchanging the models trained on miniImageNet and tieredImageNet in both Classifier-Baseline and Meta-Baseline settings. We name the model trained on miniImageNet for few-shot learning on tieredImageNet as miniImageNet→tieredImageNet, and vice versa. As shown in Table 7, Meta-Baseline + EGLayer achieves the best performance for both 1-shot (67.98%) and 5-shot (81.27%) in miniImageNet→tieredImageNet setting. In the tieredImageNet→miniImageNet setting, Classifier-Baseline + EGLayer outperforms Classifier-Baseline and Classifier-Baseline + LPLayer, improving the 1-shot by 1.04% and 0.73%, respectively. For Meta-Baseline, Meta-Baseline + EGLayer still have 1.11% and 0.89% improvements in 1-shot and 5-shot tasks. Although there is a slight decline compared to Meta-Baseline + LPLayer, our method still demonstrates an overall advantage in transfer learning tasks, validating the generalization and reliability of the

learned features.

5. Conclusions

In this paper, a novel EGLayer is introduced to enable hybrid learning, which can achieve more effective information exchange between the local deep features and a structured global knowledge graph. EGLayer is a plug-and-play module to replace the standard linear classifier, and it can significantly improve the performance of deep models by seamlessly integrating structured knowledge with data samples for deep learning. Our extensive experiments have demonstrated that our proposed hybrid learning approach with such EGLayer can greatly enhance representation learning for the tasks of cross-domain recognition and few-shot learning, and the visualization of knowledge graphs can aid in model interpretation effectively.

References

[1] Miltiadis Allamanis, Pankajan Chanthirasegaran, Pushmeet Kohli, and Charles Sutton. Learning continuous semantic representations of symbolic expressions. In *International Conference on Machine Learning*, pages 80–88. PMLR, 2017. 1

[2] Samy Badreddine, Artur d’Avila Garcez, Luciano Serafini, and Michael Spranger. Logic tensor networks. *Artificial Intelligence*, 303:103649, 2022. 1

[3] Ankan Bansal, Karan Sikka, Gaurav Sharma, Rama Chellappa, and Ajay Divakaran. Zero-shot object detection. In *Proceedings of the European Conference on Computer Vision (ECCV)*, pages 384–400, 2018. 1

[4] Jiang Bian, Bin Gao, and Tie-Yan Liu. Knowledge-powered deep learning for word embedding. In *Machine Learning and Knowledge Discovery in Databases: European Conference, ECML PKDD 2014, Nancy, France, September 15–19, 2014. Proceedings, Part I* 14, pages 132–148. Springer, 2014. 1

[5] Zhaowei Cai, Avinash Ravichandran, Subhransu Maji, Charles Fowlkes, Zhuowen Tu, and Stefano Soatto. Exponential moving average normalization for self-supervised and semi-supervised learning. In *Proceedings of the IEEE/CVF Conference on Computer Vision and Pattern Recognition*, pages 194–203, 2021. 3

[6] Riquan Chen, Tianshui Chen, Xiaolu Hui, Hefeng Wu, Guanbin Li, and Liang Lin. Knowledge graph transfer network for few-shot recognition. In *Proceedings of the AAAI Conference on Artificial Intelligence*, volume 34, pages 10575–10582, 2020. 2

[7] Wei-Yu Chen, Yen-Cheng Liu, Zsolt Kira, Yu-Chiang Frank Wang, and Jia-Bin Huang. A closer look at few-shot classification. *arXiv preprint arXiv:1904.04232*, 2019. 7

[8] Xue-Wen Chen and Xiaotong Lin. Big data deep learning: challenges and perspectives. *IEEE access*, 2:514–525, 2014. 1

[9] Yinbo Chen, Zhuang Liu, Huijuan Xu, Trevor Darrell, and Xiaolong Wang. Meta-baseline: Exploring simple meta-learning for few-shot learning. In *Proceedings of the IEEE/CVF International Conference on Computer Vision*, pages 9062–9071, 2021. 7

[10] Zhao-Min Chen, Xiu-Shen Wei, Peng Wang, and Yanwen Guo. Multi-label image recognition with graph convolutional networks. In *Proceedings of the IEEE/CVF conference on computer vision and pattern recognition*, pages 5177–5186, 2019. 2, 4

[11] Emmanuel De Bézenac, Arthur Pajot, and Patrick Gallinari. Deep learning for physical processes: Incorporating prior scientific knowledge. *Journal of Statistical Mechanics: Theory and Experiment*, 2019(12):124009, 2019. 1

[12] Andres Duque, Mark Stevenson, Juan Martinez-Romo, and Lourdes Araujo. Co-occurrence graphs for word sense disambiguation in the biomedical domain. *Artificial intelligence in medicine*, 87:9–19, 2018. 4

[13] Joan Bruna Estrach, Wojciech Zaremba, Arthur Szlam, and Yann LeCun. Spectral networks and deep locally connected networks on graphs. In *2nd international conference on learning representations, ICLR*, volume 2014, 2014. 4

[14] Chelsea Finn, Pieter Abbeel, and Sergey Levine. Model-agnostic meta-learning for fast adaptation of deep networks. In *International conference on machine learning*, pages 1126–1135. PMLR, 2017. 7

[15] Yaroslav Ganin, Evgeniya Ustinova, Hana Ajakan, Pascal Germain, Hugo Larochelle, François Laviolette, Mario Marchand, and Victor Lempitsky. Domain-adversarial training of neural networks. *The journal of machine learning research*, 17(1):2096–2030, 2016. 6, 7

[16] Junyu Gao, Tianzhu Zhang, and Changsheng Xu. I know the relationships: Zero-shot action recognition via two-stream graph convolutional networks and knowledge graphs. In *Proceedings of the AAAI conference on artificial intelligence*, volume 33, pages 8303–8311, 2019. 2

[17] Nezihe Merve Gürel, Xiangyu Qi, Luka Rimanic, Ce Zhang, and Bo Li. Knowledge enhanced machine learning pipeline against diverse adversarial attacks. In *International Conference on Machine Learning*, pages 3976–3987. PMLR, 2021. 1

[18] Will Hamilton, Zhitao Ying, and Jure Leskovec. Inductive representation learning on large graphs. *Advances in neural information processing systems*, 30, 2017. 2

[19] Kaiming He, Xiangyu Zhang, Shaoqing Ren, and Jian Sun. Deep residual learning for image recognition. In *Proceedings of the IEEE conference on computer vision and pattern recognition*, pages 770–778, 2016. 5

[20] Zhiting Hu, Xuezhe Ma, Zhengzhong Liu, Eduard Hovy, and Eric Xing. Harnessing deep neural networks with logic rules. *arXiv preprint arXiv:1603.06318*, 2016. 1

[21] Huaiibo Huang, Aijing Yu, and Ran He. Memory oriented transfer learning for semi-supervised image deraining. In *Proceedings of the IEEE/CVF conference on computer vision and pattern recognition*, pages 7732–7741, 2021. 3

[22] Michael Kampffmeyer, Yinbo Chen, Xiaodan Liang, Hao Wang, Yujia Zhang, and Eric P Xing. Rethinking knowledge graph propagation for zero-shot learning. In *Proceedings of the IEEE/CVF conference on computer vision and pattern recognition*, pages 11487–11496, 2019. 2

[23] Thomas N Kipf and Max Welling. Semi-supervised classification with graph convolutional networks. *arXiv preprint arXiv:1609.02907*, 2016. 2, 4

[24] Elyor Kodirov, Tao Xiang, and Shaogang Gong. Semantic autoencoder for zero-shot learning. In *Proceedings of the IEEE conference on computer vision and pattern recognition*, pages 3174–3183, 2017. 1

[25] Ranjay Krishna, Yuke Zhu, Oliver Groth, Justin Johnson, Kenji Hata, Joshua Kravitz, Stephanie Chen, Yannis Kalantidis, Li-Jia Li, David A Shamma, et al. Visual genome: Connecting language and vision using crowdsourced dense image annotations. *International journal of computer vision*, 123:32–73, 2017. 4

[26] Chung-Wei Lee, Wei Fang, Chih-Kuan Yeh, and Yu-Chiang Frank Wang. Multi-label zero-shot learning with structured knowledge graphs. In *Proceedings of the IEEE conference on computer vision and pattern recognition*, pages 1576–1585, 2018. 2

[27] Kwonjoon Lee, Subhransu Maji, Avinash Ravichandran, and Stefano Soatto. Meta-learning with differentiable convex optimization. In *Proceedings of the IEEE/CVF conference on computer vision and pattern recognition*, pages 10657–10665, 2019. 7

[28] Aoxue Li, Weiran Huang, Xu Lan, Jiashi Feng, Zhenguo Li, and Liwei Wang. Boosting few-shot learning with adaptive margin loss. In *Proceedings of the IEEE/CVF conference on computer vision and pattern recognition*, pages 12576–12584, 2020. 7

[29] Xiaodan Liang, Zhiting Hu, Hao Zhang, Liang Lin, and Eric P Xing. Symbolic graph reasoning meets convolutions. *Advances in neural information processing systems*, 31, 2018. 2

[30] Xiaodan Liang, Lisa Lee, and Eric P Xing. Deep variation-structured reinforcement learning for visual relationship and attribute detection. In *Proceedings of the IEEE conference on computer vision and pattern recognition*, pages 848–857, 2017. 4

[31] Yankai Lin, Zhiyuan Liu, Maosong Sun, Yang Liu, and Xuan Zhu. Learning entity and relation embeddings for knowledge graph completion. In *Proceedings of the AAAI conference on artificial intelligence*, volume 29, 2015. 4

[32] Yonggang Liu, Xiao Wang, Liang Li, Shuo Cheng, and Zheng Chen. A novel lane change decision-making model of autonomous vehicle based on support vector machine. *IEEE access*, 7:26543–26550, 2019. 4

[33] Mingsheng Long, Han Zhu, Jianmin Wang, and Michael I Jordan. Unsupervised domain adaptation with residual transfer networks. *Advances in neural information processing systems*, 29, 2016. 6, 7

[34] Nikhil Mishra, Mostafa Rohaninejad, Xi Chen, and Pieter Abbeel. A simple neural attentive meta-learner. *arXiv preprint arXiv:1707.03141*, 2017. 7

[35] Sebastian Monka, Lavdim Halilaj, Stefan Schmid, and Achim Rettinger. Learning visual models using a knowledge graph as a trainer. In *The Semantic Web–ISWC 2021: 20th International Semantic Web Conference, ISWC 2021, Virtual Event, October 24–28, 2021, Proceedings 20*, pages 357–373. Springer, 2021. 2

[36] Tsendsuren Munkhdalai, Xingdi Yuan, Soroush Mehri, and Adam Trischler. Rapid adaptation with conditionally shifted neurons. In *International Conference on Machine Learning*, pages 3664–3673. PMLR, 2018. 7

[37] Muhammad Ferjad Naeem, Yongqin Xian, Federico Tombari, and Zeynep Akata. Learning graph embeddings for compositional zero-shot learning. In *Proceedings of the IEEE/CVF Conference on Computer Vision and Pattern Recognition*, pages 953–962, 2021. 2

[38] Mohammad Norouzi, Tomas Mikolov, Samy Bengio, Yoram Singer, Jonathon Shlens, Andrea Frome, Greg S Corrado, and Jeffrey Dean. Zero-shot learning by convex combination of semantic embeddings. *arXiv preprint arXiv:1312.5650*, 2013. 2

[39] Boris Oreshkin, Pau Rodríguez López, and Alexandre Lacoste. Tadam: Task dependent adaptive metric for improved few-shot learning. *Advances in neural information processing systems*, 31, 2018. 7

[40] Pau Panareda Busto and Juergen Gall. Open set domain adaptation. In *Proceedings of the IEEE international conference on computer vision*, pages 754–763, 2017. 6, 7

[41] Zhimao Peng, Zechao Li, Junge Zhang, Yan Li, Guo-Jun Qi, and Jinhui Tang. Few-shot image recognition with knowledge transfer. In *Proceedings of the IEEE/CVF international conference on computer vision*, pages 441–449, 2019. 2

[42] Jeffrey Pennington, Richard Socher, and Christopher D Manning. Glove: Global vectors for word representation. In *Proceedings of the 2014 conference on empirical methods in natural language processing (EMNLP)*, pages 1532–1543, 2014. 4

[43] Siyuan Qiao, Chenxi Liu, Wei Shen, and Alan L Yuille. Few-shot image recognition by predicting parameters from activations. In *Proceedings of the IEEE Conference on Computer Vision and Pattern Recognition*, pages 7229–7238, 2018. 7

[44] Alec Radford, Jong Wook Kim, Chris Hallacy, Aditya Ramesh, Gabriel Goh, Sandhini Agarwal, Girish Sastry, Amanda Askell, Pamela Mishkin, Jack Clark, et al. Learning transferable visual models from natural language supervision. In *International conference on machine learning*, pages 8748–8763. PMLR, 2021. 2

[45] Mengye Ren, Eleni Triantafillou, Sachin Ravi, Jake Snell, Kevin Swersky, Joshua B Tenenbaum, Hugo Larochelle, and Richard S Zemel. Meta-learning for semi-supervised few-shot classification. *arXiv preprint arXiv:1803.00676*, 2018. 7

[46] Olga Russakovsky, Jia Deng, Hao Su, Jonathan Krause, Sanjeev Satheesh, Sean Ma, Zhiheng Huang, Andrej Karpathy, Aditya Khosla, Michael Bernstein, et al. Imagenet large scale visual recognition challenge. *International journal of computer vision*, 115:211–252, 2015. 7

[47] Andrei A Rusu, Dushyant Rao, Jakub Sygnowski, Oriol Vinyals, Razvan Pascanu, Simon Osindero, and Raia Hadsell. Meta-learning with latent embedding optimization. *arXiv preprint arXiv:1807.05960*, 2018. 7

[48] Kate Saenko, Brian Kulis, Mario Fritz, and Trevor Darrell. Adapting visual category models to new domains. In *European conference on computer vision*, pages 213–226. Springer, 2010. 5

[49] Kuniaki Saito, Shohei Yamamoto, Yoshitaka Ushiku, and Tatsuya Harada. Open set domain adaptation by backpropagation. In *Proceedings of the European conference on computer vision (ECCV)*, pages 153–168, 2018. [6](#), [7](#)

[50] Jake Snell, Kevin Swersky, and Richard Zemel. Prototypical networks for few-shot learning. *Advances in neural information processing systems*, 30, 2017. [7](#)

[51] Richard Socher, Milind Ganjoo, Christopher D Manning, and Andrew Ng. Zero-shot learning through cross-modal transfer. *Advances in neural information processing systems*, 26, 2013. [2](#)

[52] Qianru Sun, Yaoyao Liu, Tat-Seng Chua, and Bernt Schiele. Meta-transfer learning for few-shot learning. In *Proceedings of the IEEE/CVF Conference on Computer Vision and Pattern Recognition*, pages 403–412, 2019. [7](#)

[53] Flood Sung, Yongxin Yang, Li Zhang, Tao Xiang, Philip HS Torr, and Timothy M Hospedales. Learning to compare: Relation network for few-shot learning. In *Proceedings of the IEEE conference on computer vision and pattern recognition*, pages 1199–1208, 2018. [7](#)

[54] Kristina Toutanova, Xi Victoria Lin, Wen-tau Yih, Hoifung Poon, and Chris Quirk. Compositional learning of embeddings for relation paths in knowledge base and text. In *Proceedings of the 54th Annual Meeting of the Association for Computational Linguistics (Volume 1: Long Papers)*, pages 1434–1444, 2016. [4](#)

[55] Petar Veličković, Guillem Cucurull, Arantxa Casanova, Adriana Romero, Pietro Lio, and Yoshua Bengio. Graph attention networks. *arXiv preprint arXiv:1710.10903*, 2017. [2](#)

[56] Hemanth Venkateswara, Jose Eusebio, Shayok Chakraborty, and Sethuraman Panchanathan. Deep hashing network for unsupervised domain adaptation. In *Proceedings of the IEEE conference on computer vision and pattern recognition*, pages 5018–5027, 2017. [5](#)

[57] Oriol Vinyals, Charles Blundell, Timothy Lillicrap, Daan Wierstra, et al. Matching networks for one shot learning. *Advances in neural information processing systems*, 29, 2016. [7](#)

[58] Hang Wang, Minghao Xu, Bingbing Ni, and Wenjun Zhang. Learning to combine: Knowledge aggregation for multi-source domain adaptation. In *Computer Vision–ECCV 2020: 16th European Conference, Glasgow, UK, August 23–28, 2020, Proceedings, Part VIII 16*, pages 727–744. Springer, 2020. [3](#), [4](#)

[59] Xiaolong Wang, Yufei Ye, and Abhinav Gupta. Zero-shot recognition via semantic embeddings and knowledge graphs. In *Proceedings of the IEEE conference on computer vision and pattern recognition*, pages 6857–6866, 2018. [2](#)

[60] Ya Wang, Dongliang He, Fu Li, Xiang Long, Zhichao Zhou, Jinwen Ma, and Shilei Wen. Multi-label classification with label graph superimposing. In *Proceedings of the AAAI Conference on Artificial Intelligence*, volume 34, pages 12265–12272, 2020. [4](#)

[61] Han Xiao, Minlie Huang, Yu Hao, and Xiaoyan Zhu. Transg: A generative mixture model for knowledge graph embedding. *arXiv preprint arXiv:1509.05488*, 2015. [4](#)

[62] Xiaozheng Xie, Jianwei Niu, Xuefeng Liu, Zhengsu Chen, Shaojie Tang, and Shui Yu. A survey on incorporating domain knowledge into deep learning for medical image analysis. *Medical Image Analysis*, 69:101985, 2021. [1](#)

[63] Minghao Xu, Hang Wang, and Bingbing Ni. Graphical modeling for multi-source domain adaptation. *IEEE Transactions on Pattern Analysis and Machine Intelligence*, 2022. [3](#), [4](#)

[64] Kaichao You, Mingsheng Long, Zhangjie Cao, Jianmin Wang, and Michael I Jordan. Universal domain adaptation. In *Proceedings of the IEEE/CVF conference on computer vision and pattern recognition*, pages 2720–2729, 2019. [5](#), [6](#), [7](#)

[65] Jing Zhang, Zewei Ding, Wanqing Li, and Philip Ogunbona. Importance weighted adversarial nets for partial domain adaptation. In *Proceedings of the IEEE conference on computer vision and pattern recognition*, pages 8156–8164, 2018. [6](#), [7](#)

[66] Ziming Zhang and Venkatesh Saligrama. Zero-shot learning via semantic similarity embedding. In *Proceedings of the IEEE international conference on computer vision*, pages 4166–4174, 2015. [2](#)

A. Visualization

In this section, we present three graphs of the Office-31 and Office-Home datasets: the local visual graph, enhanced local graph, and global graph. Figure 4 displays these graphs, with the left column representing the results of the Office-Home dataset and the right column representing the Office-31 dataset. The first line displays the local visual graph, the second line displays the enhanced local graph, and the bottom line displays the global graph. In these graphs, thicker edges indicate stronger relations, while node size is fixed. To avoid clutter caused by too many edges, we show the top-150 edges in the Office-Home dataset and top-70 edges in the Office-31 dataset. Additionally, we have highlighted two nodes in each graph to demonstrate the differences between the three graphs.

In the Office-Home dataset, the *Scissors* node in the global graph is positioned near two types of concepts: tools and stationery. The typical tools include *Knives*, *Hammer*, and *Screwdriver*, while the stationery items include *Eraser*, *Pencil*, and *Pen*. In the local visual graph, *Scissors* is related to the typical tools category due to their similar metallic appearance. In the enhanced local graph, *Scissors* has features from both the semantic and visual graphs. Specifically, it has some thick edges with *Knives* and *Screwdriver*, as well as a thin edge with *Pen*. Another interesting node is *Mop*, which is related to *Toothbrush*, *Bucket*, *Curtains*, and other objects in the visual graph. However, in the semantic graph, it is only related to *Toothbrush*, *Bucket*, and *Sink*. As a result, in the enhanced visual graph, *Mop* is positioned closer to the semantic graph with three edges connecting it to *Toothbrush*, *Bucket*, and *Bottle*.

Table 8. Ablation study for universal domain adaptation experiments on Office-31 dataset

Methods	A→W	D→W	W→D	A→D	D→A	W→A	Average
UAN + EGLayer + σ 0.1	83.34	88.32	89.67	84.51	81.83	81.65	84.87
UAN + EGLayer + σ 0.5	18.18	18.18	18.18	9.09	16.92	17.49	16.34
UAN + EGLayer + $0.1l_1$	80.03	88.01	90.39	84.87	81.05	81.20	84.26
UAN + EGLayer + 2 layer GCN	81.16	87.71	90.91	84.01	81.76	82.01	84.59
UAN + middle EGLayer	82.55	88.70	90.91	86.09	84.14	84.11	86.08
UAN + EGLayer	83.39	92.86	94.70	84.50	87.61	86.69	88.29

In the Office-31 dataset, the *mouse* node has no edges connecting it to other nodes in the local visual graph due to its different appearance. However, it has many neighbors, including *keyboard*, *laptop computer*, and others in global graph. In the enhanced local graph, *mouse* begins to maintain some edges with other nodes, which confirms the guidance of the global graph. For *ruler*, it holds an edge with *pen* in the local visual graph, while it does not have an edge in the global graph. In the enhanced local graph, it still has an edge with *pen*, which demonstrates that visual information is preserved in the enhanced local graph.

B. Zero-Shot Learning

Table 9. Zero-shot experiments on miniImageNet and tieredImageNet

dataset	Methods	0-shot
miniImageNet	Classifier-Baseline + LPLayer	50.61 ± 0.21
	Classifier-Baseline + EGLayer	48.32 ± 0.20
tieredImageNet	Classifier-Baseline + LPLayer	49.57 ± 0.25
	Classifier-Baseline + EGLayer	48.50 ± 0.25

We conduct zero-shot experiments to assess whether our proposed method could bring extracted features closer to the semantic space by utilizing external knowledge. In these experiments, we utilize graph node embeddings instead of one-shot image features. As shown in Table 9, we observe that both LPLayer and EGLayer achieved an accuracy of around 50% in zero-shot tasks. Although LPLayer performed better in zero-shot tasks, our proposed method still has the ability to learn more robust features.

C. Ablation Studies

We conduct ablation studies on the universal domain adaptation settings using the Office-31 dataset. We perform experiments with different values of σ in Eq.9 and Eq.10, and we also use l_1 as the correlation loss, while our proposed method utilizes l_2 . These experiments are named UAN + EGLayer + σ 0.1, UAN + EGLayer + σ 0.5, and UAN + EGLayer + $0.1l_1$, respectively. Compared to our final version, all three settings show a clear drop in performance. In particular, the average performance of UAN +

EGLayer + σ 0.5 is only 16.34% due to the hard convergence of the gradient caused by a too large σ .

In addition, we also experiment with 2 GCN layers, where the first layer transfers the features to the same dimension, and the second layer aligns the features to the global graph dimension. This setting is named UAN + EGLayer + 2 layer GCN. Another setting is inserting EGLayer after the feature extractor and before the standard linear classifier as a middle layer without transferring dimensions, as our proposed EGLayer can theoretically be inserted after any layer. We named this experiment as UAN + middle EGLayer. Compared to the final version, these two settings also have a 3.7% and 2.21% average lower performance, illustrating that the final EGLayer version is simple and effective. It is noteworthy that UAN + middle EGLayer showed a 1.59% improvement in A→D domain adaptation, indicating potential for further exploration when inserting EGLayer after any layer. Therefore, we will continue to explore relevant solutions.

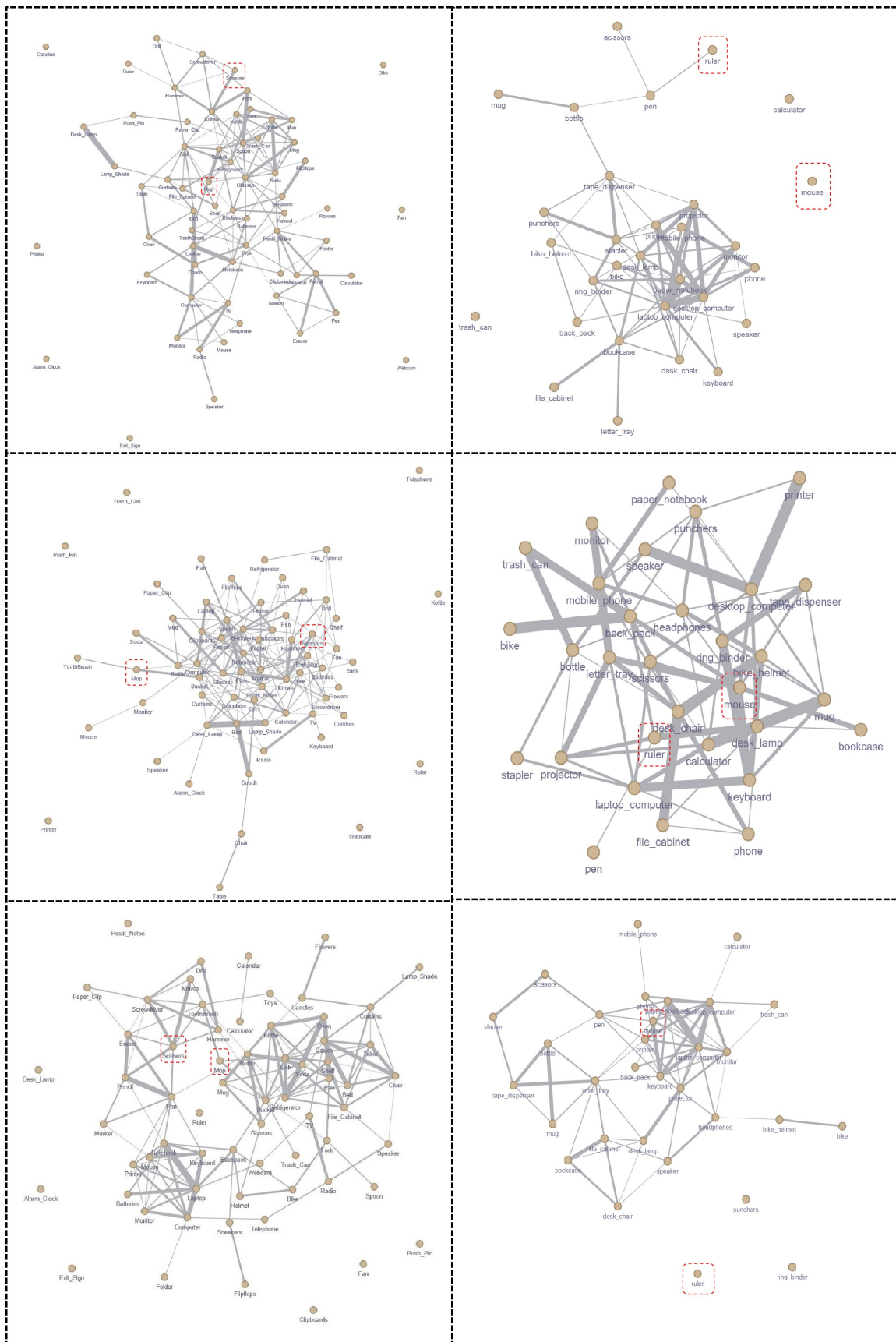


Figure 4. Visualization of three graphs.